Effect of temperature on fluidization of Geldart's group A and C powders: role of interparticle forces

F. Raganati, R. Chirone, P. Ammendola[*]

Istituto di Ricerche sulla Combustione (IRC)-CNR, Piazzale Tecchio 80, 80125 Naples, Italy

[*]Corresponding author

Tel.:+39 0817682237; fax:+39 0815936936.

E-mail address: paola.ammendola@irc.cnr.it

ABSTRACT

The interest in handling granular materials in a variety of industrial processes carried out at high temperature raises the question of how this variable affects the fluidization quality not only in the case of cohesive particles, belonging to Geldart's C powders, but also of powders classified as A. The aim of this work is, therefore, to study, from both an experimental and phenomenological point of view, the effect of temperature on the fluidization of two different powders, belonging to groups A and C of Geldart's classification. In particular, fluidization tests were performed at different temperatures (20 °C – 800 °C) and using acoustic fields of different intensities (130 – 150 dB) and frequencies (50 – 200 Hz) to highlight the influence of interparticle forces (IPFs) on the fluidization quality with increasing temperature. Pressure drops and bed expansion curves were elaborated to show the influence of temperature on minimum fluidization velocity and size of fluidized particles. Then, the validity of different correlations available in literature to predict the minimum fluidization velocity at high temperature was assessed. Finally, the experimental findings were interpreted from a phenomenological point of view on the basis of the cluster/subcluster model, which can account for temperature effects on both hydrodynamic and cohesive forces. In particular, the proposed model made it possible to directly evaluate IPFs, thus explaining the fluidization behaviour of the powders on the basis of the intensification of their cohesiveness with increasing temperature.

Keywords: Interparticle forces (IPFs); High temperature; Minimum fluidization velocity; Cluster/subcluster model; sound assisted fluidization; group A and C particles.

1. Introduction

Fluidized beds are widely used in a variety of industrial sectors for their ability to provide a high heat transfer rate and rapid solids mixing which lead to isothermal conditions in the particle bed, and high heat and mass transfer rates between gas and particles. In particular, whenever a chemical reaction employing a particulate solid as a reactant or as a catalyst requires reliable temperature control, a fluidized bed reactor is often the choice for ensuring nearly isothermal conditions by suitable selection of the operating conditions[1]. Therefore, the interest in handling granular materials in various industrial processes carried out at thermal levels above ambient conditions raises the question of how temperature affects the fluidization quality not only in the case of cohesive particles, which belong to Geldart's C powders[2], but also of powders classified as A[2].

According to different works reported in literature[3–5], some peculiar phenomena, happening at elevated temperatures, cannot be merely explained in light of the influence of temperature on the properties of the fluidizing gas (density and viscosity)[6]. The approach based solely on considering such changes in the gas properties is valid under the condition that only hydrodynamic forces (HDFs) control the fluidization behaviour. On the contrary, a different approach must be used when, besides these hydrodynamic forces, also interparticle forces (IPFs) are simultaneously active. Therefore, in light of these considerations, it must be taken into account that temperature remarkably affects not only the gaseous phase but also the solid phase, considered as variations in the interparticle forces. Among all the possible types of interparticle forces, mainly van der Waals, electrostatic and capillary forces are the most significant ones. Briefly, concerning the effect of temperature on interparticle forces other than van der Waals ones, the electrostatic forces generally decrease with increasing temperature until they can be considered negligible[7]. The same goes for capillary forces, since with increasing temperature regardless of all other factors, they decrease with the condensation of water vapor becomes more and more difficult[7]. Besides the above-mentioned types on particle interactions, also the forces arising from sintering can play an important role in

particle adhesion[7]. More specifically, sintering is a time-dependent process occurring in the quiescent zones in which interparticle motion is limited, i.e. the time in the quiescent zones should be sufficiently long for sinter necks to reach a critical size such that the aggregates formed are sufficiently strong not to be fractured by the gas flow[8]. Only in this case agglomerates will tend to segregate at the bottom of the bed and will sinter together (i.e. the sinter neck of sufficient becomes permanent resisting the breakage forces due to the movement of solids and gas) thus eventually lead to defluidisation[9]. In other words, whether the sintering leads to a real bonding of particles depends on whether the particles are disturbed before a proper sintering bond can be formed.

With reference to van der Waals attractive forces, they are affected by temperature through the Hamaker constant and the hardness of the material, which can be both dependent on this variable[10]. The hardness of the material, it is only slightly affected by an increase of temperature, unless the materials and temperatures are not close to the melting point or to the sintering conditions. Regarding the Hamaker constant, there is still controversy in the specialized literature surrounding the effect of temperature. Visser[3] reported a modest variation in the case of two water drops in vacuum, and also show some experimental results for a water-hydrocarbon system. Similarly, in their discussion of van der Waals forces, Dzyaloshinskii, Lifshitz, and Pitaevskii mention that the effect of temperature on the interaction of two bodies is 'usually completely unimportant'[11]. On the contrary, Krupp[12] and Kerminen[13] founded a strong dependency with the temperature. Likewise, Castellanos et al.[14] provided a report on the temperature dependence of the Hamaker constant for fluorocarbon compounds.

In this framework, the influence of interparticle forces on fluidization behaviour has been suggested by various Authors[1,15,16]. Formisani et al.[15] indicated the increase in interparticle forces as the cause for temperature-dependence of particulate phase voidage and minimum fluidization velocity (u_{mf}). Lettieri et al.[1] also found that the fluidization behaviour of different types of materials belonging to the A group of Geldart's classification can be dominated by interparticle

forces when temperature is increased. In particular, they clearly demonstrated how the effect of temperature increase could cause the transition from a group A to a group C type of behaviour. Also Geldart and Wong[16] found a transition group, i.e. slightly cohesive group A powders, possessing some of the features of the cohesive group C powders and group A powders. They used for these "semi-cohesive" powders the designation group AC. Even though no direct evidence on the effect of interparticle forces on fluidization behaviour has been proved, there is a general consideration that they may play a role also in the case of groups A materials when temperature is increased.

The aim of this work is, therefore, to characterize and describe, from both an experimental and phenomenological point of view, the effect of temperature on the fluidization of two different powders, belonging to groups A and C of Geldart's classification. Sound assisted fluidization, which is capable of hindering the IPFs, has been used to highlight the influence of IPFs on the fluidization quality with increasing temperature. Then, the level of the predictivity of different correlations available in literature for the evaluation minimum fluidization velocity also at high temperature was assessed. Finally, the cluster/subcluster model[17,18], capable of accounting for temperature effects on both hydrodynamic and cohesive forces, was applied to interpret the experimental findings, regarding the effect of an increase of temperature on the fluidization quality of group A and C powders, from a phenomenological point of view.

2. Experimental

2.1 Materials

Two different materials were used in this work: ashes collected at the exit of a fluidized bed combustor and a silica sand powder. Both the powders were characterized from a granulometric point of view. In particular, their particle size distributions were obtained by using a laser granulometer (Master-sizer 2000 Malvern Instruments), after the dispersion of the powders in water under mechanical agitation of the suspension and with the application of ultrasound (US). This system allows detection of particles in the range of 0.02 - 2000 μm. Then, the average diameter of

the powders was determined from the granulometric distribution. In particular, the Sauter mean diameter was evaluated, i.e. the surface-volume diameter defined as the diameter of a sphere having the same ratio of external surface to volume as the particle.

The properties of both the powders are reported in Table 1. In particular, the ashes belong to the C group of Geldart's classification[2]. Even though, based on its properties, the silica sand can be classified as a group A powder, it is characterized by a quite broad size distribution, having particles as small as few microns.

2.2 Experimental apparatus and procedure

The experimental apparatus used is shown in Fig. 1. It consists of a fluidized bed column made of a Quartz (40 mm ID and 1500 mm high) and equipped with Pyrex gas distributor plate (porosity grade 3) located at 300 mm from the bottom of the column. The section of the column below the gas distributor acts as wind-box: it is filled with Quartz rings, thus maximizing the uniformity of the gas flow entering the fluidized bed. This solution provides a good dispersion of the fluidizing gas, thus limiting fluidization troubles due to the formation of preferential channels, namely the feed of the fluidizing gas through a limited number of points. In addition, this section of the reactor also acts as a pre-heating chamber for the fluidizing gas. The column is provided with a pressure probe located at the wall, 5mm above the gas distributor, to measure the pressure drops across the bed.

The sound-generation system consists of a digital signal generator, a power audio amplifier rated up to 40W and a 8W woofer loudspeaker. The acoustic field is introduced inside the column through an purpose-designed sound wave guide located at the top of the freeboard[19–21]. The sound wave guide was properly designed to prevent the elutriated powders from dirtying the loudspeaker and also to protect the loudspeaker from the irradiation of the bed[19–21]. This experimental set-up was also designed according to the Helmholtz resonator, i.e. one of the most used engineering noise control methods, in order to reduce the sound insulation even for high intensity acoustic fields[19–21].

A type K thermocouple (Chromel-Alumel) vertically inserted inside the bed is used to monitor

the temperature inside the bed at different radii. A temperature controller is used to monitor the bed temperature during the experimental tests and keep it at the desired value. A heating jacket (Tyco Thermal Controls GmbH) is wrapped around its external surface to heat the column to the desired temperature. In particular, it has been purpose-designed: it is 500mmhigh with an isothermal height of 350 mm and it is also provided with a window, which allows the fluidization quality and bed expansion to be visually assessed.

Gas feed is prepared using N_2 cylinders (99.995%) in order to prevent any intensification of the powder cohesiveness due to air moisture and the flowrates were set and controlled by two mass flow controllers (Brooks 8550S). Beds made of 180 and 80 g were used for Group A and C materials, respectively, in order to have same bed heights (about 10 cm).

Pressure drops and bed expansion curves as a function of gas velocity were measured in fluidization experiments carried out at different temperatures (20 °C – 800 °C) and using acoustic fields of different intensities (130 – 150 dB) and frequencies (50 – 200 Hz). In particular, for each test, pressure drop curves were obtained measuring the pressure drops by both decreasing (DOWN) and increasing (UP) the superficial gas velocity. curves. Then, experimental data were worked out to calculate the main fluidization parameters. No noticeable differences were obtained between UP and DOWN. However, all the results shown hereafter were obtained from the DOWN curves. In particular, the minimum fluidization velocity (u_{mf}) was evaluated from pressure drops data according to a graphical procedure (i.e. as intersection between the line fitting the data for flow through a packed bed, and a horizontal line fitting the data for the fully fluidized bed)[22]; the bed voidage at u_{mf} (ε_{mf}) was evaluated from the bed height data at u_{mf} as $\varepsilon_{mf} = 1 - (m/\rho_p)/(H_{mf}A)$, being m the mass of particle loaded in the fluidization column, ρ_p the particle density, H_{mf} the bed height at u_{mf} and A the cross sectional area of the fluidization column; the average size of fluidized particles (d_p) was evaluated from the experimental values of u_{mf}, using the correlation proposed by Wen and Yu[23] and considering an apparent density for aggregates lower than the density of the

primary particles.

3. Literature correlation predictivity

The value of u_{mf} is usually determined experimentally by measuring the pressure drop as a function of gas velocity. It can also be predicted using several equations available in the specialized literature. All these correlations were developed based on the data of non-cohesive particles, thus meaning that IPFs have not been taken into account. For this reason, they may be not suitable for fine particles wherein IPFs are relatively strong compared with gravity. Moreover, these can be generally divided in two main categories, depending on whether or not their application requires the knowledge of the bed voidage at the minimum fluidization velocity and the particle sphericity.

Among those requiring the prior evaluation of these parameters, the most comprehensive is derived from the Ergun equation[24]. Using an extensive set of experimental data covering a wide range of particle size and shapes, Ergun presented a general equation to calculate the pressure drop across a packed bed for all flow conditions (laminar to turbulent). Then, setting this equation equal to the gravitational force of the particle bed, the minimum fluidization velocity can be calculated:

$$Ar = 150\frac{(1-\varepsilon_{mf})}{\varepsilon_{mf}^3\Phi^2}Re_{mf} + \frac{1.75}{\varepsilon_{mf}^3\Phi}Re_{mf}^2 \quad (1)$$

where Ar is the Archimedes number $\left(d_p^3\rho(\rho_p-\rho)g/\mu^2\right)$, Re_{mf} is the Reynolds number evaluated at u_{mf} $\left(\rho u_{mf} d_p/\mu\right)$, μ and ρ are the gas viscosity and density, respectively, and d_p, ρ_p and Φ are the size, density and sphericity (or shape factor) of the particles, respectively. The particle size used in the Sauter mean diameter of the powder.

This equation combines both the laminar and turbulent components of the pressure drops across a particle bed. In laminar flow conditions the first component of the equation dominates and the viscous forces are predominant, whereas, under turbulent flow conditions the second component of the Ergun equation dominates and the inertia forces are predominant. Therefore, the following correlations can be obtained in the case of fine (Eq. 2) and coarse particles (Eq. 3), respectively:

$$u_{mf} = \frac{d_p^2(\rho_p-\rho)}{150\mu}\frac{\varepsilon_{mf}^3\Phi^2}{1-\varepsilon_{mf}} \qquad \mathrm{Re_{mf}} < 20 \qquad (2)$$

$$u_{mf}^2 = \frac{d_p(\rho_p-\rho)g}{1.75\rho}\varepsilon_{mf}^3\Phi \qquad \mathrm{Re_{mf}} > 1000 \qquad (3)$$

As stated above, the main drawback of this approach is that both ε_{mf} and Φ can hardly be determined. The importance of ε_{mf} is clear from Eq. 1 and 2. Indeed, a 10% error in the determination of ε_{mf} results in a 38% and 15% error on u_{mf} in the case of laminar and turbulent flow, respectively[25]. ε_{mf} is function of the shape and rugosity of the particles, and it generally decreases with increasing d_p. Typically, it is indirectly evaluated from the experimental bed expansion curves.

Just to eliminate the explicit dependence of u_{mf} on these difficult-to-evaluate parameters, many researchers proposed modified equations, starting from the Ergun equation. In this framework, Wen and Yu[23] and Leva[26] proposed Eq. 4 and 5, respectively:

$$Re_{mf} = [33.7^2 + 0.0408Ar]^{0.5} - 33.7 \qquad (4)$$

$$u_{mf} = \frac{d_p^{1.82}\rho(\rho_p-\rho)^{0.94}g}{\mu^{0.88}\rho^{0.06}} \qquad (5)$$

3.1 Effect of temperature

All the above-mentioned equations were obtained on the basis of experiments performed at room temperature. Therefore, they do not implicitly include the effect of temperature on u_{mf}. Indeed, predictions of u_{mf} at high temperature are essentially based on the application of these correlations by introducing the dependence on the temperature of the gas density and viscosity. In particular, gas density is inversely proportional to the absolute temperature (T). On the contrary, the viscosity of a gas is proportional to T^n, where n usually varies in the range 0.5 - 1.0. So, as temperature increases, gas density decreases and gas viscosity increases. This combined effect, related to changes in density and viscosity, results in a decrease in the Archimedes number when temperature is increased. However, how this affects u_{mf} is not trivial. In this framework, according to Yates[27], the

correlations obtained at ambient temperature can still be used at high temperatures when variations of density and viscosity of gas and a correct value of the minimum fluidization voidage are used. In particular, assuming a gas viscosity dependence on the square root of temperature, he showed that: i) for Group A particles, an increase in temperature results in a decrease in u_{mf}, although the effect is relatively modest; ii) for B Group materials, u_{mf} increases with increasing temperatures when the inertial term (in which the gas density appears) is prevailing, whereas, it decreases when the viscous term begins to become dominant. Experimental evidences of these trends were also given by other Authors[25,28].

However, all Authors agree in highlighting the importance of choosing the correct value of ε_{mf} to be used in the Ergun equation. With reference to this point, the (direct or indirect) effect of the temperature on ε_{mf} is not yet fully clarified. Although few Authors[29] suggest that ε_{mf} is independent of temperature, except for possible "buoyancy" phenomena associated with gas feeding at temperature lower than that of the bed (i.e. ε_{mf} determined at low temperature can be used in traditional correlations to make predictions at high temperatures), most of the Authors, according to Botterill et al.[25], claim that ε_{mf} does vary with temperature. In particular, for small particles, ε_{mf} increases with increasing temperatures and it tends to become constant at high temperatures. On the contrary, for larger particles, ε_{mf} has a non-monotonic trend, since it first decreases with increasing temperatures and then increases. Finally, for even larger particles ε_{mf} is practically constant with the temperature. Therefore, u_{mf} at high temperature can be predicted using the available literature correlations (e.g. Ergun equation), simply using the value of ε_{mf} evaluated at the temperature in question. Obviously, all the equations, which do not have explicit dependence on the ε_{mf} (e.g. Wen and Yu[23] and Leva[26] equation), cannot take into account the variability of ε_{mf} with the temperature.

4. Cluster/sub-cluster model

The cluster/subcluster oscillator model, originally proposed by Russo et al.[17] to describe the

fluidization of cohesive powders (i.e. belonging to group C of Geldart's classification), was used in this work to justify and explain the effect of temperature on the fluidization quality of both group C and A powders from a phenomenological point of view by directly evaluating the intensity of IPFs.

Russo et al.[17] interpreted the break-up of agglomerated solids in sound-assisted fluidization on the basis of two distinct physical phenomena: the hydrodynamic stresses due to gas flowing and the cohesivity of the agglomerated solids, which in turn depends both on the packing of primary particles within the agglomerate and on the strength of the elementary interparticle interaction[17].

The main assumptions of the model are the following[17].

The existence of elastic forces between clusters and subclusters, active at the contact points, was assumed. In other words, according to this model, an elastic behaviour of the whole cluster-subcluster structure occurs as a result of the elasticity of the interparticle contacts. In particular, elastic forces are of the type kx, where k is the elastic constant relative to the force acting at each contact point between a cluster and a subcluster and x the vertical displacement of the subcluster relative to the cluster. A subcluster is in contact with the cluster at n points, so that the overall elastic constant is [nk]. The number of contact points is proportional to the external surface area of the subcluster.

The cohesive frictional force, F_c, between a cluster and a subcluster is given by[30]:

$$F_c = n\mu F_{cw} \quad (6)$$

where $\mu = 0.1$ is a static friction coefficient[30] and F_{cw} is the van der Waals force along straight lines through centers of a cluster and a subcluster[17]. Even though electrostatic, capillary and van der Waals forces may develop at contact points between solids[17], only van der Waals forces are considered in the model. Electrostatic forces are disregarded because of the low velocity at which the powder has been fluidized. Capillary forces are neglected considering the low humidity of the fluidizing gas. The cohesive frictional force tends to keep the subcluster in place.

A subcluster detaches from the cluster when the elastic force [nk]x (i.e., the force that, would be

necessary to keep together cluster and subcluster) is larger than the cohesive frictional force F_c, i.e. if the disaggregating force due to the application of the acoustic field, F_{sound}, is larger than the cohesive force F_c:

$$F_{sound} \geq F_c \Rightarrow [nk]|x| \geq n\mu F_{cw} \quad (7)$$

The balance of forces acting on the subcluster, taking into account inertial, elastic and drag forces, is given by:

$$m\frac{d^2x}{dt^2} + [nk]x - c_{ds}\left(U\sin(2\pi ft) - \frac{dx}{dt}\right) = 0 \quad (8)$$

being m the mass of the subcluster, U the amplitude of the air particle velocity, f the sound frequency and c_{ds} the drag force per unit gas velocity. In particular, the difference $\left(U\sin(2\pi ft) - \frac{dx}{dt}\right)$ is the slip velocity between the gas and the subcluster, whereas c_{d_s} is given by:

$$c_{d_s} = 3\pi\beta\nu\rho d_p \quad (9)$$

where ν and ρ are the kinematic viscosity and the density of the gas, respectively, d_p is the subcluster diameter and β = 1.7 is a correction factor accounting for the influence of neighboring clusters [31].

Then, integration of Eq (8) leads to[30]:

$$x(t) = \frac{U}{2\pi\sqrt{f^2 + \left(\frac{2\pi m}{c_{d_s}}\right)^2 \left(f_n^2 - f^2\right)^2}}\sin(2\pi ft + \varphi) = A(f)\sin(2\pi ft + \varphi) \quad (10)$$

where, A is the amplitude of the displacement of the subcluster relative to the cluster, φ is the phase lag between the velocity of the gas and the displacement of the subcluster, f is the sound frequency and f_n is the natural frequency of the undamped oscillator given by[17]:

$$f_n = \frac{1}{2\pi}\sqrt{\frac{[nk]}{m}} = \frac{1}{2\pi}\sqrt{\frac{[nk]}{(\pi/6)\rho_s d_p^3}} \quad (11)$$

Then, the peak of the A(f) curve occurs at the frequency f_0 which is the resonance frequency of the damped oscillator given by:

$$f_0 = f_n\left(1 - \left(\frac{c_{d_s}}{4\pi f_n m}\right)^2\right)^{0.5} \quad (12)$$

Combining Eq (11) and Eq. (12), the overall elastic constant [nk] can be expressed as a function of f_0:

$$[nk] = (2\pi)^2\left(f_0^2 + 2\left(\frac{c_{d_s}}{4\pi m}\right)^2\right)m \quad (13)$$

The value of the disaggregating force, F_{sound}, i.e. the force generated by sound application, was evaluated by applying the failure conditions, given by Eq (7). Therefore, F_{sound} is the disaggregating force that is necessary for subclusters of size d_p^* to detach from clusters. d_p^* was evaluated from experimental data as the size of subclusters obtainable at the maximum response frequency, f_0^*, i.e. the frequency at which, for given sound intensity (SPL), subclusters of minimum size d_p^* detach from clusters. The maximum response frequency is the counterpart of f_0, i.e. the resonance frequency of the subcluster behaving like a damped forced oscillator, namely $f_0 = f_0^*$.

The occurrence of the failure condition implies a tangency condition

$$[n^*k]A(f) = n^*\mu F_{cw} \quad (14)$$

Being n^* the number of active contact points between the subcluster of size d_p^* and the cluster it detaches from. Namely, F_{sound} can be evaluated using a graphical procedure as the maximum of the curve of the elastic force. In particular, the curve of the elastic force, $[n^*k]$ $A(f)$, can be plotted as a function of sound frequency. Then, the failure condition implies that the horizontal line corresponding to the cohesive forces ($n^*\mu F_{cw}$), which is independent of the sound frequency, is tangent to the maximum of the curve of elastic force. This procedure can be used to obtain the disaggregating force directly, overcoming the lack of knowledge of the number of active contact points n^*.

The same procedure was used to evaluate the cohesiveness of the powder, F_{cohes}, defined as the force that would be necessary to break the clusters down to the nominal size of the powders, i.e. the Sauter diameter. In particular, the same equations used for F_{sound} were applied, but considering d_p^*

equal to the Sauter diameter.

This model is capable of accounting for the effect of temperature on both F_{sound} and F_{cohes}. Indeed, temperature affects gas density and viscosity, which directly influence the drag force acting on particle clusters (Eq. 8). In particular, temperature directly affects both the drag force per unit gas velocity, c_{ds} (Eq. 9), and the air particle velocity, U, i.e. the propagation of the acoustic wave in the medium. Moreover, temperature also indirectly affects the size of the actual fluidizing structures, i.e. the size d_p^* of the subclusters detached from the cluster, which was experimentally evaluated at each investigated temperature.

5. Results and discussion

5.1 Experimental results

5.1.1 Group A powder – Silica sand

Fig. 2 reports the experimental trends obtained for u_{mf}, ε_{mf} and d_p, as a function of sound intensity and frequency at the different investigated temperatures (20 - 600 °C). The values obtained under ordinary fluidization conditions were also reported as comparison. It is clear that, the application of the sound generally results in a sensible decrease of u_{mf} (Figs. 2a and b) and d_p (Figs. 2c and d) with respect to the tests performed without the application of any acoustic fields, for each investigated temperature. This experimental evidence is revealing of the occurrence of aggregation phenomena, i.e. the fluidizing entities are not the original particles but the particle aggregates. Therefore, the "effective d" of the fluidizing structures is the size of the particle aggregates. This can be explained referring to the granulometric distribution of the powders, which is characterized by the presence of both coarser (< 100 μm) and finer (< 30 μm) particles with respect to the Sauter diameter of the distribution (Table 1). This means that, even at ambient temperature, the powder is characterized by a certain grade of cohesiveness, given by the adhesion of the finer particles to other particles and

giving birth to agglomerated structures (clusters), due to the action of IPFs. As a matter of fact, under ordinary conditions the actual size of the fluidizing structures is always larger than the Sauter diameter of the powder (Table 1), i.e. the size of the primary particles. In other words, under ordinary conditions the fluidizing structures are remarkably larger than those fluidizing under sound assisted conditions. In this framework, as largely reported in the specialized literature[22,32–34], the application of the sound is capable to hinder IPFs, thus promoting an efficient break-up of the clusters yielded by cohesive forces into smaller structures (i.e. smaller d_p), thus causing a consequence reduction of u_{mf} (since the fluidizing entities are smaller).

With reference to the effect of the sound parameters, it is also evident that they play a crucial role. In particular, in line with several works reported in literature[22,32–34], SPL has a beneficial effect on the fluidization quality. Indeed, d_p (Fig. 2c) and u_{mf} (Fig.2 a), as a consequence, are always decreased passing from 130 to 150 dB. This evidence is due to the fact that with increasing SPLs more energy is introduced inside the bed, thus making the break-up of larger clusters more and more efficient. Indeed, the gap between the size of the granulometric distribution and the actual size of the fluidizing aggregates decrease with increasing SPLs. In particular, for temperatures up to 200°C, SPLs as high as 150 dB are capable of disrupting clusters down to size comparable to the Sauter diameter of the powder.

With reference to the effect of sound frequency, also in agreement to indications reported in literature[22,32–34], it has a non-monotonic effect on the fluidization quality (i.e. a nonlinear relationship is observed between all the fluidization parameters and the sound frequency). Indeed, the curves of d_p (Fig. 2d) and u_{mf} (Fig. 2b), as a consequence, are characterized by a minimum value at 120 Hz, i.e. the maximum response frequency (f_0^*). This behavior is due to the fact that the frequency directly affects the relative motion between clusters and subclusters, which, in turn, promotes the essential break-up and reaggregation mechanism. In particular, for too high frequencies the acoustic field cannot properly propagate inside the bed; the sound absorption

coefficient is proportional to the square of sound frequency as sound propagates through the bed of particles[17]. Consequently, for too high sound frequencies, most of the acoustic energy is absorbed by the upper part of the bed (since the sound source is located at the top of the column), whereas, only an attenuated sound energy reaches the bed bottom, thus failing to efficiently disrupt large agglomerates at the bottom of the bed and, hence, fluidization quality decreases (i.e. u_{mf} increases)[35]. On the contrary, for too low frequencies the relative motion between larger and smaller sub-aggregates is practically absent[22,32–34]. In particular, the period of the acoustic excitation is long with respect to the time needed for the flow of fluidizing gas to set up local channeling in the bed, which, after the initial perturbation, has recovered its adhesion[35].

With reference to ε_{mf}, the analysis of Figs. 2e and f shows that the application of the sound results in a general slight decrease of ε_{mf} with respect to the values obtained under ordinary conditions. This experimental evidence is in agreement with indications reported in literature on the compaction of the bed under sound assisted fluidization conditions[22]. With reference to the effect of SPL, its increase generally result in a reduction of εmf (Fig. 2e) due to the intensification of the above-mentioned compaction phenomena. In line with the results obtained for u_{mf} and d_p, sound frequency shows a non-monotonic effect also on ε_{mf} (Fig. 2f).

With reference to the effect of temperature, the acoustic field becomes less efficient with increasing temperatures until its effect becomes negligible for the highest temperature (600 °C), i.e. no differences were observed between ordinary and sound assisted tests. In particular, values of u_{mf}, d_p and ε_{mf} as a functions of the bed temperature are shown in Fig. 3, in order to better highlight the effect of this variable on the fluidization parameters. It is clear that all the parameters increase with temperature under both ordinary and sound assisted fluidization conditions. The increasing trend of ε_{mf} is in line with several works reporting its variation with the temperature due to changes in fluid-dynamics of the system as the temperature is increased[25]. On the contrary, the increasing trend of u_{mf} is in contrast with indications reported in literature for group A particles, for which an increase

in temperature results in a decrease in u_{mf} [27]. As discussed in the introduction section, this behaviour is not expected on the basis of purely hydrodynamic considerations on the effect of temperature on gas viscosity and density since also IPFs are simultaneously active, and they become more and more intense as temperature is increased. As a matter of fact, the intensification of IPFs is responsible of the formation of larger fluidizing structures, i.e. higher values of d_p (Figs. 3c and d) with increasing temperatures. In other words, the cohesiveness of the powder is enhanced at higher temperatures and more and more particles sticks together to form larger clusters. As a consequence, higher values of u_{mf} were obtained passing from 20 to 600 °C. Therefore, the growing trend of u_{mf} with temperature can only result from an increase of IPFs with the temperature.

As a further confirmation of the enhanced cohesive character of the powder with the temperature, the difference observed between ordinary and sound assisted conditions tends to decrease increasing the bed temperature from 20 °C to 600 °C. At this temperature no noticeable differences were obtained between the test performed under ordinary and sound assisted conditions. In other words, the capability of the of the acoustic perturbation in hindering IPFs becomes lower and lower as the temperature is increased, until it eventually vanishes for bed temperature of 600 °C. In particular, as clearly inferable from Figs. 3c and d, even an optimal acoustic field of 150 dB – 120 Hz keeps its effectiveness up to 200 °C. Indeed, the break-up mechanism is actually effective only up to 200 °C, since the fluidizing aggregates are disrupted down to the Sauter diameter. On the contrary, for temperatures higher than 200 °C, the break-up mechanism becomes more and more ineffective, until it becomes negligible at 600 °C, at which the actual fluidizing aggregates is roughly two times the Sauter diameter of the powder.

5.1.2 Group C powder – Ashes

Fig. 4 reports the experimental trends obtained for u_{mf}, ε_{mf} and d_p, under sound assisted fluidization conditions (at a fixed SPL of 150 dB) as a function of sound frequency (f) at the different investigated temperatures (20 - 800 °C). The values under ordinary fluidization conditions

could not be reported since no fluidization regime could be achieved without the application of any acoustic field since channeling and plugging phenomena were observed. In line with indications reported in literature[22,32–34] and with the results obtained for the silica sand, sound frequency has a non-monotonic effect on the fluidization quality, as confirmed by the fact that the curve of d_p (Fig. 4b) and u_{mf} (Fig. 4a), as a consequence, is characterized by a minimum value at 120 Hz, i.e. the optimal frequency (f_0^*). Even though the application of the sound makes it possible to actually achieve a fluidization state of the powder, not even SPLs as high as 150 dB with an optimal frequency of 120 Hz are capable of disrupting the particle clusters down to the average size of the powder (Table1). This result confirms the highly cohesive character of the tested material.

An increase of the bed temperature causes an increase of all the fluidization parameters, u_{mf}, ε_{mf} and d_p (Fig. 5). This is due an intensification of IPFs which makes the powder more and more difficult to be fluidized. As a matter of fact, the break-up mechanism, yielded by the application of the acoustic fields, becomes less effective as the temperature is increased: at 800 °C the actual size of the fluidizing clusters is roughly fifteen times the Sauter diameter of the powder. This is clearly shown in Fig. 5 b, in which it is evident that, whatever the sound frequency, the gap between the actual size of the fluidizing structures and the average size of the powder, i.e. its Sauter diameter, becomes larger passing from 20 to 800 °C.

5.2 Literature correlation predictivity

Experimental values of u_{mf}, obtained for the A and C group powders with and without the use of acoustic fields, were compared with values predicted by correlations available in literature accounting for the variation of gas density and viscosity with temperature. Ergun[24], Wen and Yu[36], and Leva[26] correlations were applied using the Sauter mean diameter of the powder as particle size to be inserted in the equations. In particular, in the case of the Ergun equation, i.e. the only one requiring the knowledge of ε_{mf}, u_{mf} was calculated making two different hypotheses: i) assuming that ε_{mf} does not vary with the temperature, according to Pattipatti et al.[29]; ii) assuming that ε_{mf} is a

function of the temperature, according to Botterill et al.[25]. In the former case, a constant value, obtained at ambient temperature, was adopted (ε_{mf} = const.); in the latter, a different value, obtained from experiments, is considered for each temperature ($\varepsilon_{mf} = \varepsilon_{mf}(T)$).

Figs. 6a and b reports the comparison between the predicted and experimental values of u_{mf} obtained for the silica sand in the tests performed under ordinary and sound assisted conditions, respectively.

The analysis of the graph reported in Fig. 6a clearly shows that that the shape/magnitude of the experimental values of u_{mf} do not follow the shape/magnitude predicted by the literature correlations. In particular, the predicted values of u_{mf} are always lower than the experimental ones. Only when experimental values of ε_{mf} evaluated at the different temperatures are used, i.e. considering the dependence of ε_{mf} on temperature, predictions approaches the experimental data from the magnitude point of view. However, the shape, i.e. the trend, is still not right, since all literature correlations provide a decreasing trend of u_{mf} with temperature, even when experimental ε_{mf} values have been taken into account. Experimental values, on the contrary, show an increasing trend with the temperature, due to the enhanced cohesiveness of the powder as temperature is increased. Therefore, literature correlations do not provide the right trend of u_{mf} with the temperature, even when the "correct" ε_{mf} value is used. In general, their poor predictivity is mainly due to the fact that they consider implicitly negligible the effect of IPFs, which ultimately are the main cause of relatively high values of ε_{mf} and of the formation of aggregates capable of being fluidized as pseudo-particles.

The importance of the role played by IPFs is confirmed by the fact that the application of a proper acoustic field (150 dB – 120 Hz) to hinder their action results in a general improvement of the correlations predictivity, as clearly shown in Fig. 6b. In particular, at least for temperatures lower than 400 °C, the values of u_{mf} appear to be well predicted by all the considered correlations. This is probably explained considering that the actual size of the fluidizing structures is far more similar to

that of the original particle distribution than in the case of ordinary fluidization tests. With reference the trend of u_{mf} with temperature, only the correlation taking into account that $\varepsilon_{mf} = \varepsilon_{mf}$ (T) is capable of predicting an increasing trend of u_{mf} with temperature. On the whole, the predictivity of all the equations is enhanced, at least in terms of absolute magnitude of u_{mf}, when applied to experimental data from sound assisted fluidization tests; and when also the variability of ε_{mf} is taken into account the predictivity is good also in terms of trend. The still not perfect accuracy of the prediction (i.e. experimental value lower than predicted ones) is likely due to the fact that at higher temperatures IPFs, even though hindered by the application of an intense acoustic field, are not yet fully balanced.

As regards group C powder, the correlation predictivity is always very poor, as clearly shown in Fig. 7, even though sound assisted conditions and dependence of ε_{mf} with temperature are considered. Indeed, even at ambient temperature the predicted values of u_{mf} are more than three times the values obtained experimentally. Since the powder in question has a strong cohesive character (as typical of materials belonging to the C group powders), even at low temperatures the acoustic field is not capable of completely balance the IPFs. This is confirmed by the fact that not even at ambient temperature the fluidizing aggregates are broken down to the average size of the granulometric distribution (Table 1). This means that the acoustic wave is only capable of partially hindering the cohesiveness of the material, which actually makes it possible to achieve a fluidization state of the powder in the form of clusters as large as seven times its Sauter diameter. Obviously, the beneficial effect played by the acoustic field becomes less significant with increasing temperatures, since the cohesiveness of the powder is strongly enhanced. As a consequence, fluidizing aggregates reach dimension up to fifteen times the average size of the powder (Table 1) at 800 °C and, therefore, a further dramatic drop can be observed in the predictivity of the literature correlations (Fig. 7).

5.3 Model results

The cluster/subcluster model was applied for A and C group powders, in order to analyze and explain the experimental effect of temperature on the fluidization parameters on the basis of the increasing intensity of IPFs. In particular, the application of the model, which can account for temperature effects on both hydrodynamic and cohesive forces, make it possible to directly evaluate the frictional cohesive forces F_{sound}, thus explaining and clarifying the experimental findings also from a phenomenological point of view.

The values of F_{sound} evaluated from the model are reported in Figs. 8a and b as a function of the bed temperature for A and C group powders, respectively. The values of the cohesiveness of the materials, F_{cohes}, i.e. the force that would be necessary to break the clusters down to the nominal size of the powders, are also reported (solid lines). It is clear that both the disaggregating force exerted by the applied acoustic field, which counteracts IPFs, and IPFs become larger as temperature is increased. This occurrence is essentially due to the combined changes in the fluidizing gas properties. In particular, increasing temperatures lead to a decrease of gas density and an increase of gas viscosity, which directly influence the drag force acting on particle clusters (Eq. 8). Indeed, temperature directly affects both the drag force per unit gas velocity, c_{ds} (Eq. 9), and the propagation of the acoustic wave in the medium. In particular, the air particle velocity, U, increases with increasing temperatures, thus resulting in a consequent increase of the overall velocity of gas impacting on clusters. However, even though increasing temperatures result in the enhancement of the force exerted by the acoustic field, F_{sound}, its actual disaggregating action becomes less effective. This is because the difference between the value of the force theoretically needed to fully balance IPFs, F_{cohes}, and the actual F_{sound} tends to increase as temperature is increased. This is because F_{sound} depends on the actual size of the fluidizing aggregates, whereas F_{cohes} was calculated using the Sauter diameter of the powder. As a consequence, F_{sound} tends to become lower than F_{cohes} with increasing temperatures, since at higher temperatures the acoustic field is not still capable of disrupting the clusters down to the Sauter diameter of the powder. Indeed, as obtained from the

experimental results, the average size of the fluidizing aggregates and, in turn, u_{mf} increase with increasing temperatures.

With reference to the group A silica sand, it is clear that F_{sound} is increased with increasing values of SPL (Fig. 8a), thus explaining the experimental results shown in Figs. 2a and c. Indeed, increasing SPL from 130 to 150 dB results in a decrease of the fluidizing subcluster size, and therefore in a decrease of u_{mf}, since more energy is introduced inside the bed, thus making the break-up mechanism more efficient. Moreover, regarding the influence of temperature, F_{sound} is nearly equal to F_{cohes} for temperatures up to 200 °C, thus meaning that the acoustic field is actually effective in completely hindering IPFs, as discussed in the previous sections. On the contrary, for higher temperatures (> 200 °C) the difference between F_{sound} and F_{cohes} become more and more noticeable. This explains the loss of effectiveness of the acoustic field application which results in a significant increase of the fluidizing aggregate size and, consequently, u_{mf} (Figs. 3a and c).

Likewise, regarding the group C powder (Fig. 8b), the difference between F_{sound} and F_{cohes} is noticeable even at ambient temperature, F_{cohes} being roughly threefold F_{sound}. This explains why sound assisted fluidization, even though making possible the achievement of an actual fluidization regime through the break-up and reaggregation mechanism of fluidizing clusters, is, however, not capable of disrupting these clusters down to the size of the original particles (Fig. 5b).

6. Conclusions

The effect of temperature on the fluidization of two different powders, belonging to groups A and C of Geldart's classification, was studied from both an experimental and phenomenological point of view. In particular, the different role played by interparticle forces on fluidization of group A and C powders was highlighted by comparing experimental findings obtained from ordinary and sound assisted fluidization tests. Pressure drops and bed expansion curves were elaborated to show the influence of temperature on minimum fluidization velocity, size of fluidized particles and bed

voidage. The results obtained showed that an increase of the bed temperature causes an increase of all the above-mentioned fluidization parameters.

Then, the actual predictivity at high temperature of different correlations available in literature for the evaluation of the minimum fluidization velocity was assessed. The results obtained showed that the behaviour of both group A and C powders can hardly be explained on a purely hydrodynamic basis, i.e. considering the sole effect of temperature on gas viscosity and density. Indeed, deviations of literature correlations increase with temperature for both A and C group powders, whereas decrease when cohesive forces are hindered (i.e. when acoustic fields are applied).

Finally, the experimental findings were interpreted from a phenomenological point of view on the basis of the cluster/subcluster model. In particular, the proposed model, capable of accounting for temperature effects on both hydrodynamic and cohesive forces, made it possible to directly evaluate IPFs. Therefore, the fluidization behaviour of the powders was explained on the basis of the intensification of their cohesiveness with increasing temperature.

7. References

(1) Lettieri, P.; Newton, D.; Yates, J. G. High Temperature Effects on the Dense Phase Properties of Gas Fluidized Beds. *Powder Technol.* **2001**, *120*, 34.

(2) Geldart, D. Types of Gas Fluidization. *Powder Technol.* **1973**, *7*, 285.

(3) Visser, J. Van Der Waals and Other Cohesive Forces Affecting Powder Fluidization. *Powder Technol.* **1989**, *58*, 1.

(4) Wu, S. Y.; Baeyens, J. Effect of Operating Temperature on Minimum Fluidization Velocity. *Powder Technol.* **1991**, *67*, 217.

(5) Shabanian, J.; Chaouki, J. Hydrodynamics of a Gas-Solid Fluidized Bed with Thermally Induced Interparticle Forces. *Chem. Eng. J.* **2015**, *259*, 135.

(6) Baerns, M. Effect of Interparticle Adhesive Forces on Fluidization of Fine Particles. *Ind. Eng. Chem. Fundam.* **1966**, *5*, 508.

(7) Seville, J. P. K.; Willett, C. D.; Knight, P. C. Interparticle Forces in Fluidisation: A Review. *Powder Technol.* **2000**, *113*, 261.

(8) Seville, J. P. K.; Silomon-Pflug, H.; Knight, P. C. Modelling of Sintering in High Temperature Gas Fluidisation. *Powder Technol.* **1998**, *97*, 160.

(9) Knight, P. C.; Seville, J. P. K.; Kamiya, H.; Horio, M. Modelling of Sintering of Iron Particles in High-Temperature Gas Fluidisation. *Chem. Eng. Sci.* **2000**, *55*, 4783.

(10) Xu, C.; Zhu, J.-X. Effects of Gas Type and Temperature on Fine Particle Fluidization. *China Particuology* **2006**, *4*, 114.

(11) Dzyaloshinskii, I. E.; Lifshitz, E. M.; Pitaevskii, L. P. The General Theory of van Der Waals Forces. *Adv. Phys.* **1961**, *10*, 165.

(12) Krupp, H. Particle Adhesion Theory and Experiment. *Adv. Colloid Interface Sci.* **1967**, *1*, 111.

(13) Kerminen, V.-M. Simulation of Brownian Coagulation in the Presence of van Der Waals Forces and Viscous Interactions. *Aerosol Sci. Technol.* **1994**, *20*, 207.

(14) Castellanos, A. J.; García-Sucre, M.; Urbina-Villalba, G. Temperature Dependence of Hamaker Constants for Fluorocarbon Compounds.

(15) Formisani, B.; Girimonte, R.; Pataro, G. The Influence of Operating Temperature on the Dense Phase Properties of Bubbling Fluidized Beds of Solids. *Powder Technol.* **2002**, *125*, 28.

(16) Geldart, D.; Wong, A. C. Y. Fluidization of Powders Showing Degrees of Cohesiveness—II.

Experiments on Rates of De-Aeration. *Chem. Eng. Sci.* **1985**, *40*, 653.

(17) Russo, P.; Chirone, R.; Massimilla, L.; Russo, S. The Influence of the Frequency of Acoustic Waves on Sound-Assisted Fluidization of Beds of Fine Particles. *Powder Technol.* **1995**, *82*, 219.

(18) Chirone, R.; Raganati, F.; Ammendola, P.; Barletta, D.; Lettieri, P.; Poletto, M. A Comparison between Interparticle Forces Estimated with Direct Powder Shear Testing and with Sound Assisted Fluidization. *Powder Technol.,* **2018**, *323*, 1.

(19) Raganati, F.; Ammendola, P.; Chirone, R. Effect of Acoustic Field on CO_2 Desorption in a Fluidized Bed of Fine Activated Carbon. *Particuology* **2015**, *23*, 8.

(20) Raganati, F.; Ammendola, P.; Chirone, R. CO_2 Capture Performances of Fine Solid Sorbents in a Sound-Assisted Fluidized Bed. *Powder Technol.* **2014**, *268*, 347.

(21) Ammendola, P.; Raganati, F.; Chirone, R. Effect of Operating Conditions on the CO_2 Recovery from a Fine Activated Carbon by Means of TSA in a Fluidized Bed Assisted by Acoustic Fields. *Fuel Process. Technol.* **2015**, *134*, 494.

(22) Ammendola, P.; Chirone, R.; Raganati, F. Fluidization of Binary Mixtures of Nanoparticles under the Effect of Acoustic Fields. *Adv. Powder Technol.* **2011**, *22*, 174.

(23) Wen, C. Y.; Yu, Y. H. A Generalized Method for Predicting the Minimum Fluidization Velocity. *AIChE J.* **1966**, *12*, 610.

(24) Ergun, S. Fluid Flow Through Packed Columns. *Chem. Eng. Prog.* **1952**, *48*, 89.

(25) Botterill, J. S. M.; Y, T.; Yuregir, K. R. The Effect of Temperature on Fluidized Bed Behaviour. *Chem. Eng. Commun.* **1982**, *15*, 227.

(26) Leva, M. *Fluidization*; McGraw-Hill: New York, 1959.

(27) Yates, J. G. Effects of Temperature and Pressure on Gas-Solid Fluidization. *Chem. Eng. Sci.* **1996**, *51*, 167.

(28) Raso, G.; D'Amore, M.; Formisani, B.; Lignola, P. G. The Influence of Temperature on the Properties of the Particulate Phase at Incipient Fluidization. *Powder Technol.* **1992**, *72*, 71.

(29) Pattipati, R. R.; Wen, C. Y. Minimum Fluidization Velocity at High Temperatures. *Ind. Eng. Chem. Process Des. Dev.* **1981**, *20*, 705.

(30) Flugge, W. *Handbook of Engineering Mechanics*, McGrawHill: New York, 1963.

(31) O'Neill, M. E. A Sphere in Contact with a Plane Wall in a Slow Linear Shear Flow. *Chem. Eng. Sci.* **1968**, *23*, 1293.

(32) Ammendola, P.; Chirone, R.; Raganati, F. Effect of Mixture Composition, Nanoparticle Density and Sound Intensity on Mixing Quality of Nanopowders. *Chem. Eng. Process. Process Intensif.* **2011**, *50*, 885.

(33) Raganati, F.; Ammendola, P.; Chirone, R. Role of Acoustic Fields in Promoting the Gas-Solid Contact in a Fluidized Bed of Fine Particles. *KONA Powder Part. J.* **2015**, *32*, 23.

(34) Ammendola, P.; Chirone, R. Aeration and Mixing Behaviours of Nano-Sized Powders under Sound Vibration. *Powder Technol.* **2010**, *201*, 49.

(35) Valverde, J. M.; Raganati, F.; Quintanilla, M. a. S.; Ebri, J. M. P.; Ammendola, P.; Chirone, R. Enhancement of CO_2 Capture at Ca-Looping Conditions by High-Intensity Acoustic Fields. *Appl. Energy* **2013**, *111*, 538.

(36) Wen, C. Y.; Yu, Y. H. Mechanics of Fluidization. *Chem. Eng. Prog. Symp. Ser.* **1966**, *62*,

100.

Figure caption

Fig. 1. Experimental apparatus: (1) N2 cylinder; (2) flow meter; (3) mass flow controller; (4) 40mm ID fluidization column; (5) microphone; (6) sound guide; (7) wind-box; (8) pressure transducer; (9) loudspeaker; (10) stack; (11) thermocouple; (12) temperature controller; (13) heating jacket.

Fig. 2. Silica Sand (A group) - Effect of SPL on (a) u_{mf}, (c) d_p and (e) ε_{mf} at a fixed frequency (120 Hz) and at different temperatures; effect of frequency on (b) u_{mf}, (d) d_p and (f) ε_{mf}, at a fixed SPL (150 dB) and at different temperatures.

Fig. 3. Silica Sand (A group) - Effect of temperature on (a) u_{mf}, (c) d_p and (e) ε_{mf} at a fixed frequency (120 Hz) and at different SPLs; effect of temperature on (b) u_{mf}, (d) d_p and (f) ε_{mf}, at a fixed SPL (150 dB) and at different frequencies.

Fig. 4. Ashes (C group) - Effect of frequency on (a) u_{mf}, (b) d_p and (c) ε_{mf}, at a fixed SPL (150 dB) and at different temperatures.

Fig. 5. Ashes (C group) - Effect of temperature on (a) u_{mf}, (b) d_p and (c) ε_{mf} at a fixed SPL (150 dB) and at different frequencies.

Fig. 6. Silica Sand (A group) - Comparison between experimental and predicted values of u_{mf} for (a) ordinary and (b) sound assisted tests (150 dB – 120 Hz).

Fig. 7. Ashes (C group) - Comparison between experimental and predicted values of u_{mf}. SPL = 150 dB, f = 120 Hz.

Fig. 8. Effect of temperature on the disaggregating force exerted by the sound (F_{sound}) and on the cohesiveness (F_{cohes}) of (a) silica sand and (b) ashes.

Figures

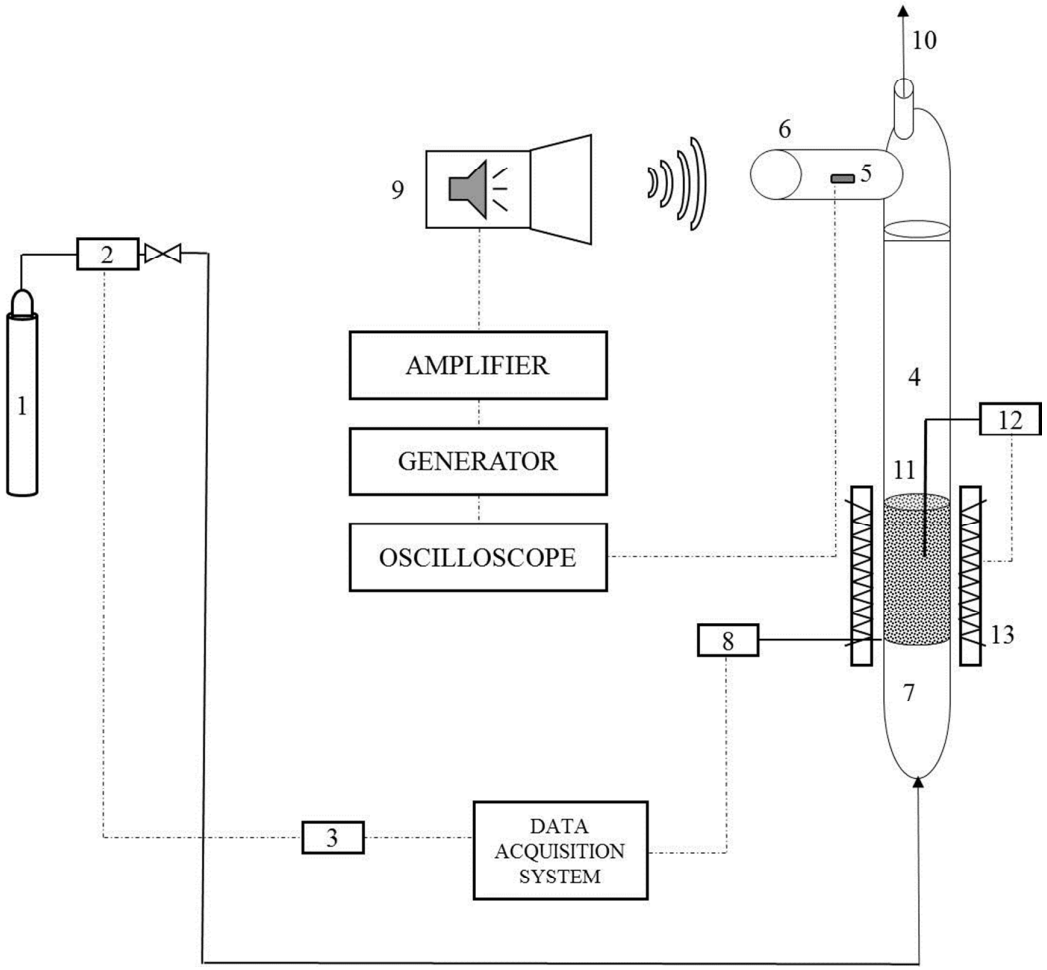

Fig. 1. Experimental apparatus: (1) N2 cylinder; (2) flow meter; (3) mass flow controller; (4) 40mm ID fluidization column; (5) microphone; (6) sound guide; (7) wind-box; (8) pressure transducer; (9) loudspeaker; (10) stack; (11) thermocouple; (12) temperature controller; (13) heating jacket.

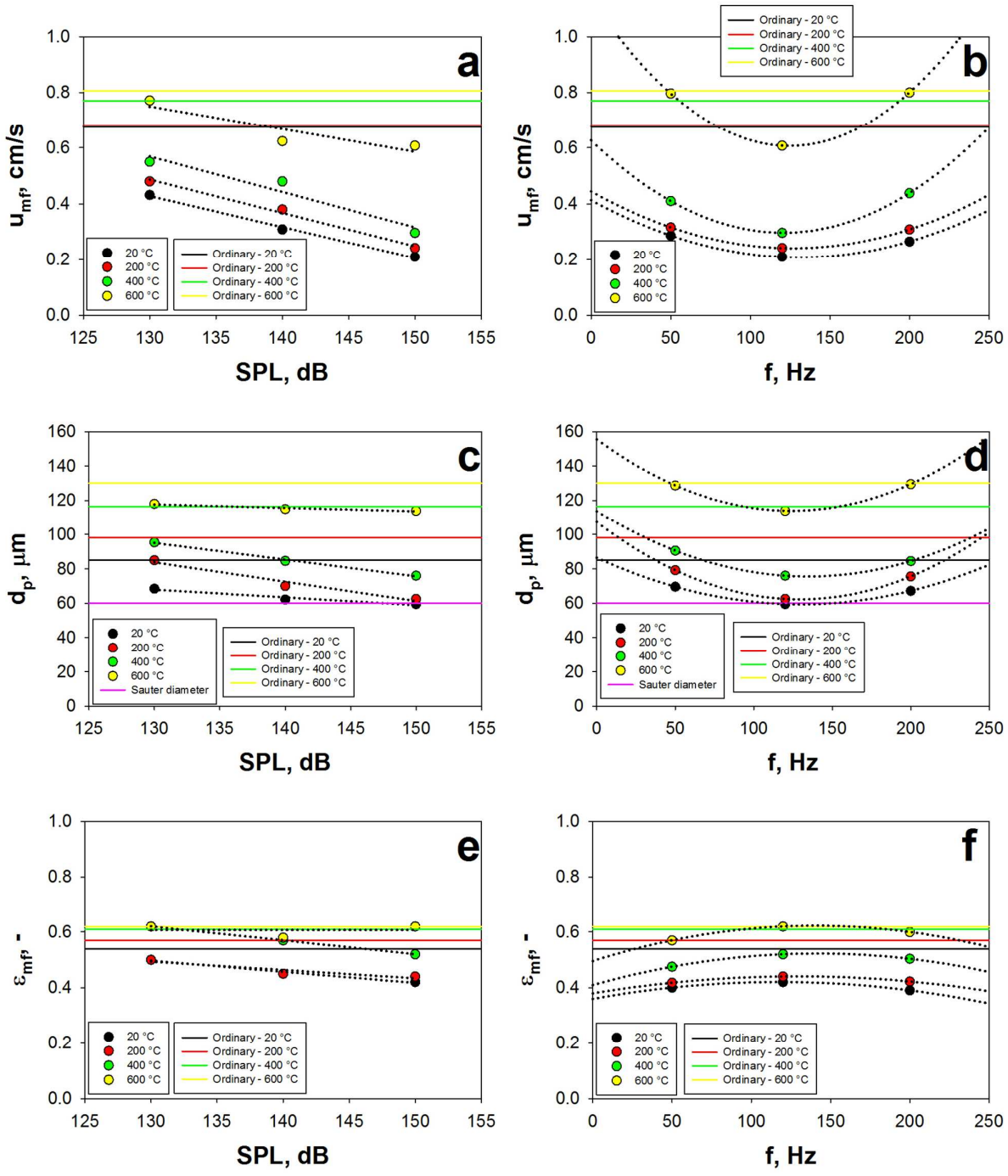

Fig. 2. Silica Sand (A group) - Effect of SPL on (a) u_{mf}, (c) d_p and (e) ε_{mf} at a fixed frequency (120 Hz) and at different temperatures; effect of frequency on (b) u_{mf}, (d) d_p and (f) ε_{mf}, at a fixed SPL (150 dB) and at different temperatures.

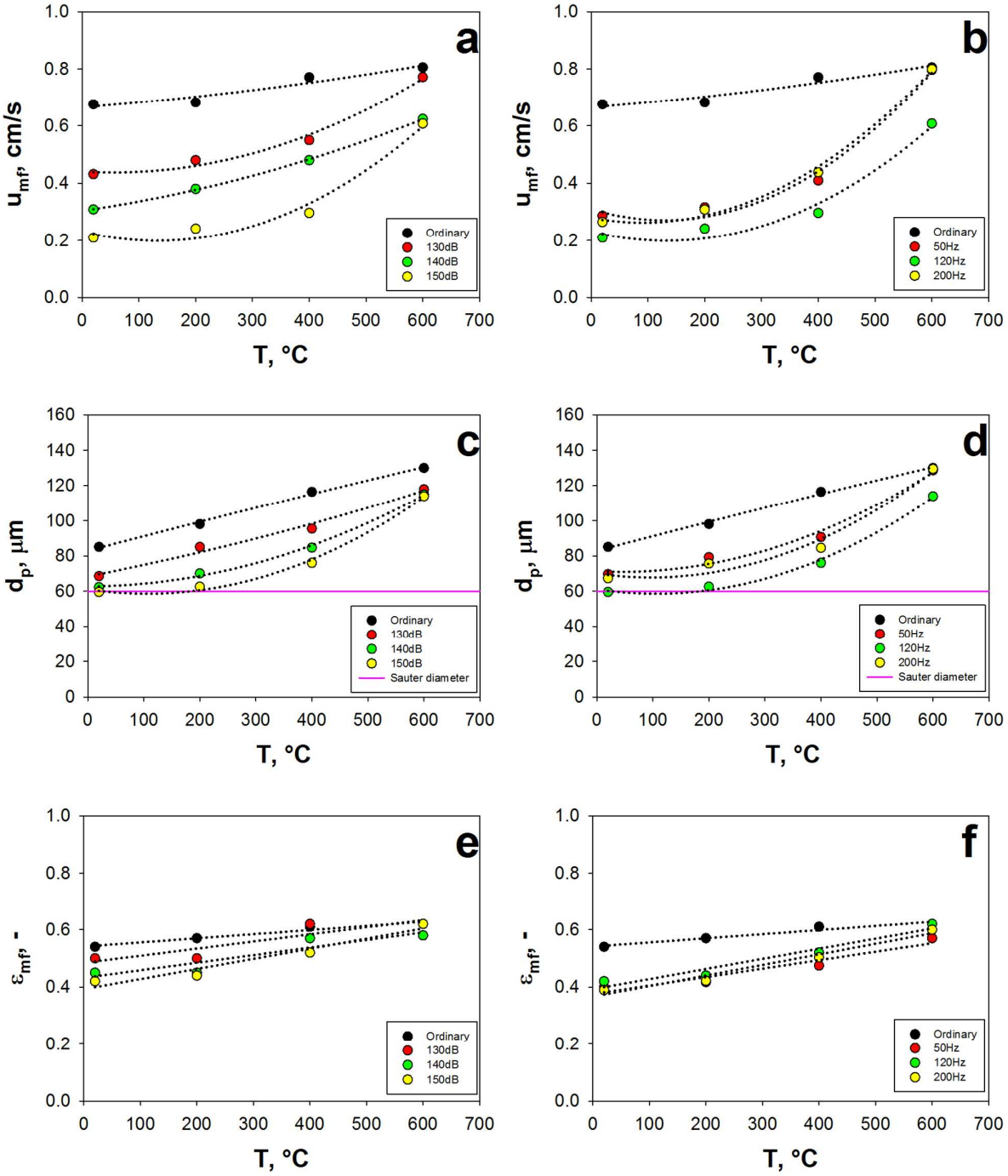

Fig. 3. Silica Sand (A group) - Effect of temperature on (a) u_{mf}, (c) d_p and (e) ε_{mf} at a fixed frequency (120 Hz) and at different SPLs; effect of temperature on (b) u_{mf}, (d) d_p and (f) ε_{mf}, at a fixed SPL (150 dB) and at different frequencies.

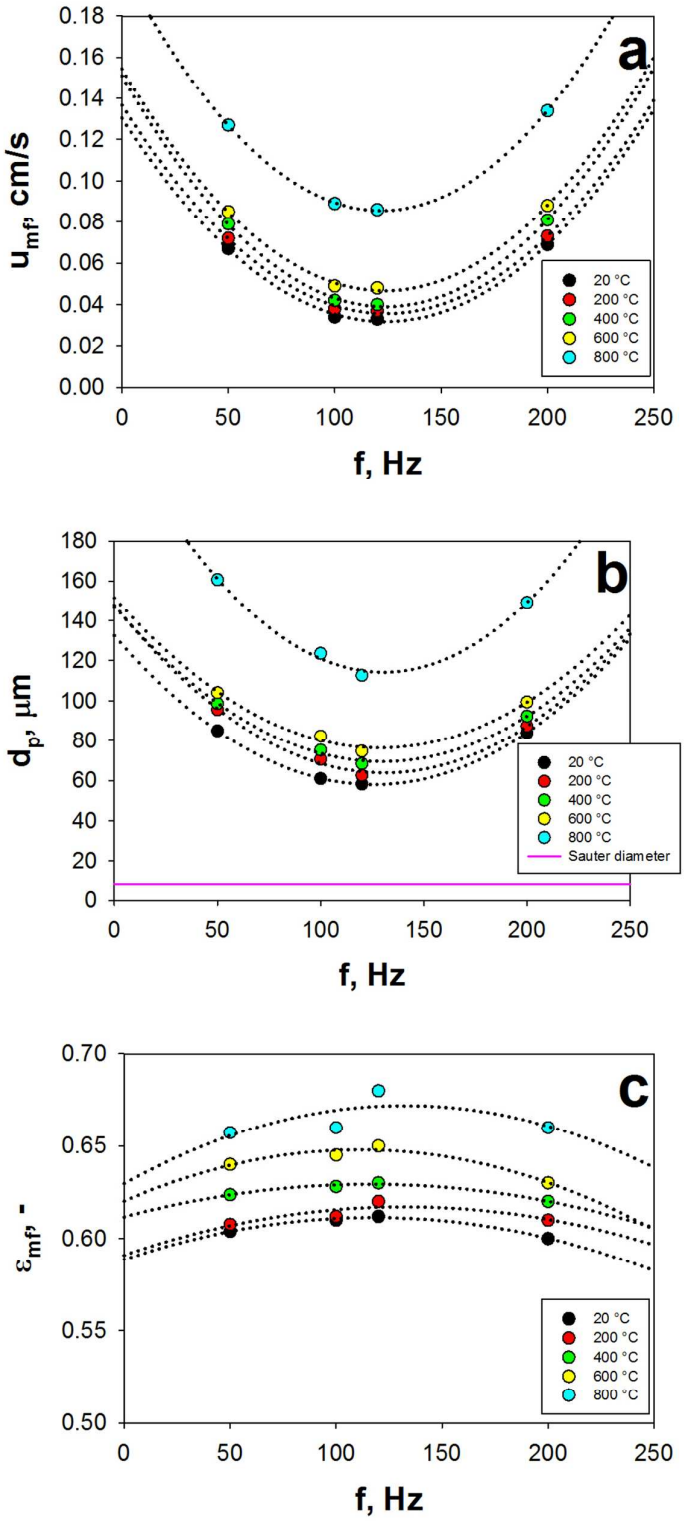

Fig. 4. Ashes (C group) - Effect of frequency on (a) u_{mf}, (b) d_p and (c) ε_{mf}, at a fixed SPL (150 dB) and at different temperatures.

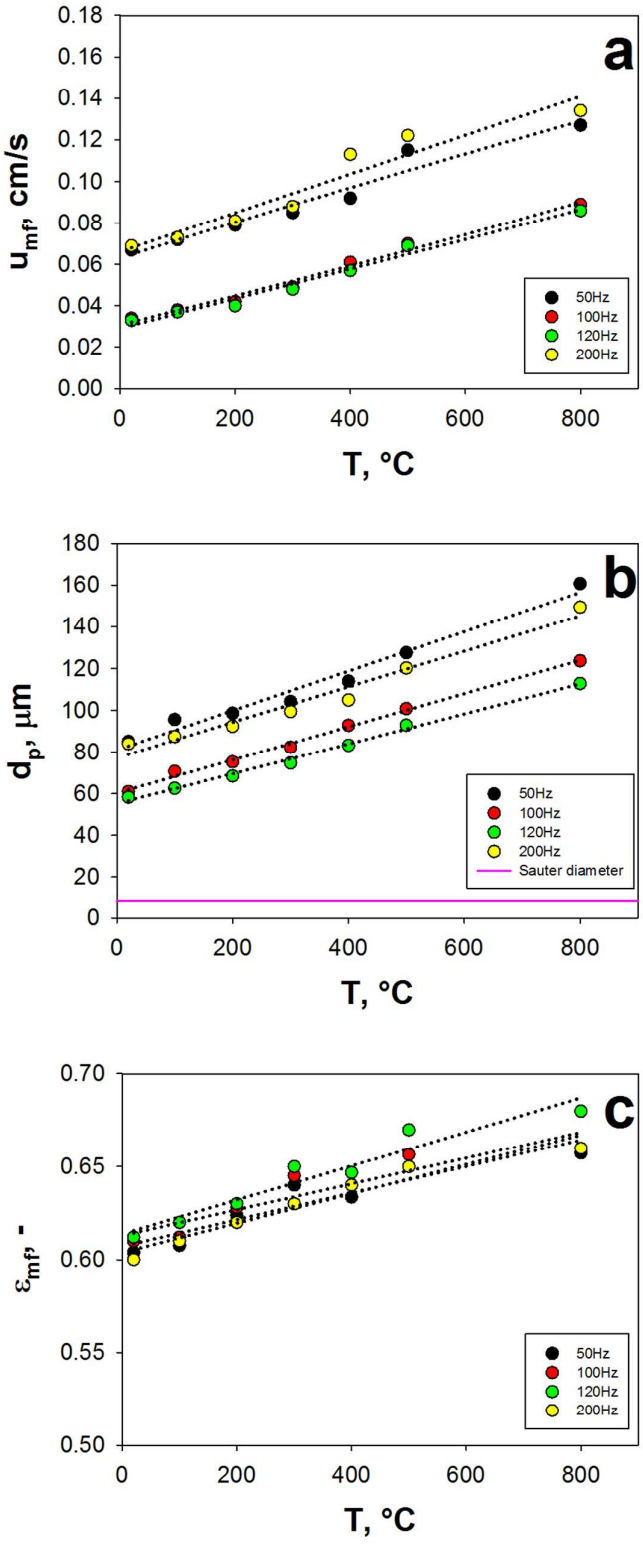

Fig. 5. Ashes (C group) - Effect of temperature on (a) u_{mf}, (b) d_p and (c) ε_{mf} at a fixed SPL (150 dB) and at different frequencies.

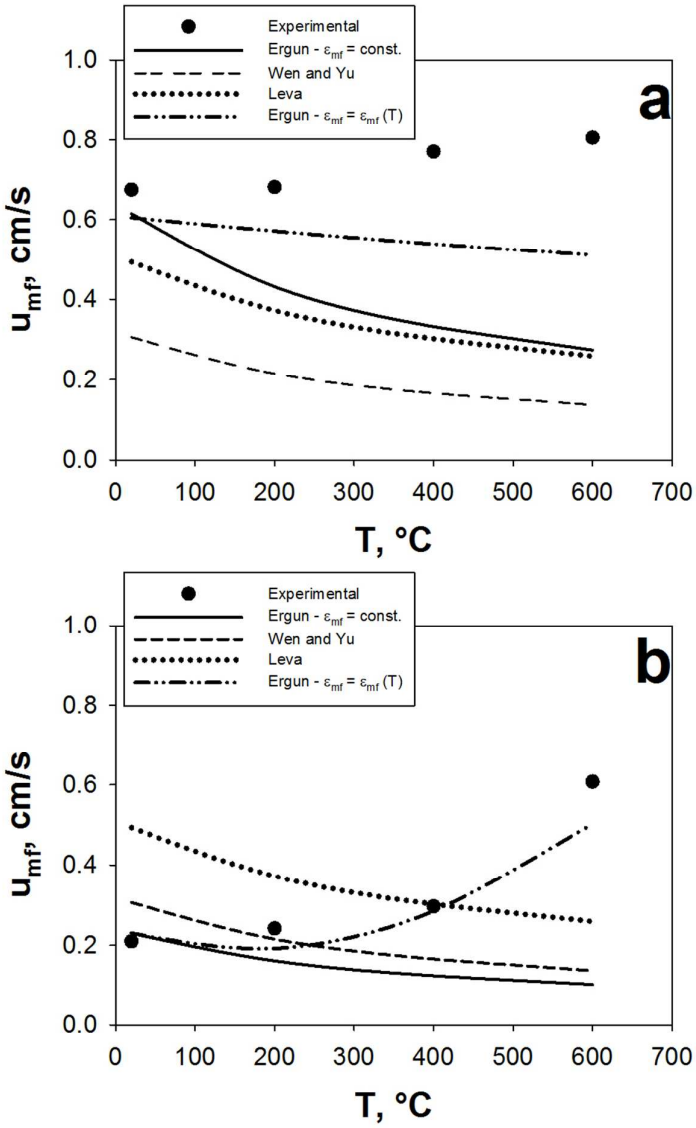

Fig. 6. Silica Sand (A group) - Comparison between experimental and predicted values of u_{mf} for (a) ordinary and (b) sound assisted tests (150 dB – 120 Hz).

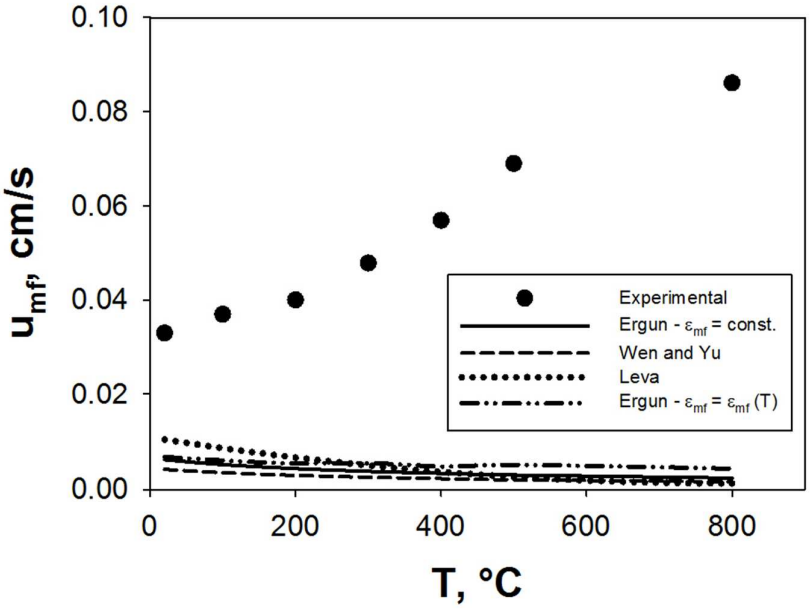

Fig. 7. Ashes (C group) - Comparison between experimental and predicted values of u_{mf}. SPL = 150 dB, f = 120 Hz.

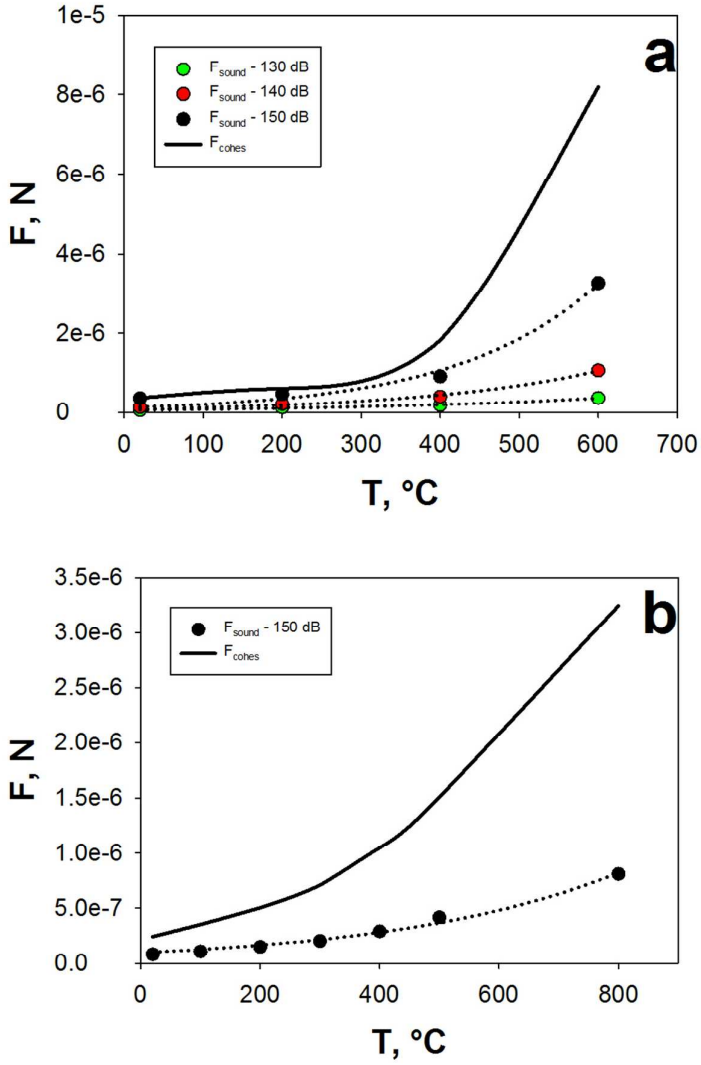

Fig. 8. Effect of temperature on the disaggregating force exerted by the sound (F_{sound}) and on the cohesiveness (F_{cohes}) of (a) silica sand and (b) ashes.

Tables

Table 1. Properties of the tested powders.

	Ashes	Silica sand
Particle nominal size, μm	< 60	6-146
Sauter diameter, μm	8	60
Apparent density, kg/m^3	2000	2600
Sphericity factor, -	0.5	0.73
Gerdart Classification	C	A

For Table of Contents Only